PAPER

Fluorescence labelled XT5 modified nano-capsules enable highly sensitive myeloma cells detection

View the article online for updates and enhancements.

Fluorescence labelled XT5 modified nano-capsules enable highly sensitive myeloma cells detection

Araz Norouz Dizaji[1,2,*] [iD], **Matin Yazdani Kohneshahri**[1,3,7], **Sena Gafil**[2,7], **Muhammed Tilahun Muhammed**[4], **Tulin Ozkan**[5], **Ilyas Inci**[6] [iD], **Cengiz Uzun**[1] **and Esin Aki Yalcin**[2,*]

[1] Department of Chemistry, Faculty of Science, Hacettepe University, 06800-Ankara, Turkey
[2] Department of Pharmaceutical Chemistry, Faculty of Pharmacy, Ankara University, Ankara, Turkey
[3] Gelisim Medikal, Tibbi malz. Paz. San ve Tic. Ltd Sti, Ankara, Turkey
[4] Suleyman Demirel University, Department of Pharmaceutical Chemistry, Faculty of Pharmacy, Isparta, Turkey
[5] Department of Medical Biology, School of Medicine, Ankara University, Ankara, Turkey
[6] Izmir Democracy University, Vocational School of Health Services, Department of Dentistry Services, Dental Prosthetics Technology, Izmir–35140, Turkey

E-mail: araz.norouz@hacettepe.edu.tr and esin.aki@ankara.edu.tr

Abstract

Accurate diagnosis of cancer cells in early stages plays an important role in reliable therapeutic strategies. In this study, we aimed to develop fluorescence-conjugated polymer carrying nanocapsules (NCs) which is highly selective for myeloma cancer cells. To gain specific targeting properties, NCs, XT5 molecules (a benzamide derivative) which shows high affinity properties against protease-activated receptor-1 (PAR1), that overexpressed in myeloma cancer cells, was used. For this purpose, 1,2-distearoyl-sn-glycero-3-phosphoethanolamine-N-[carboxy (polyethylene glycol)-2000]-carboxylic acid ($DSPE-PEG_{2000}-COOH$) molecules, as a main encapsulation material, was conjugated to XT5 molecules due to esterification reaction using N,N′-dicyclohexylcarbodiimide as a coupling agent. The synthesized $DSPE-PEG_{2000}-COO-XT5$ was characterized by using FT-IR and ^1H NMR spectroscopies and results indicated that XT5 molecules were successfully conjugated to $DSPE-PEG_{2000}-COOH$. Poly(fluorene-alt-benzothiadiazole) (PFBT) conjugated polymer (CP) was encapsulated with $DSPE-PEG_{2000}-COO-XT5$ due to dissolving in tetrahydrofuran and ultra-sonication in an aqueous solution, respectively. The morphological properties, UV–vis absorbance, and emission properties of obtained CP encapsulated $DSPE-PEG_{2000}-COO-XT5$ (CPDP-XT5) NCs was determined by utilizing scanning electron microscopy, UV–vis spectroscopy, and fluorescent spectroscopy, respectively. Cytotoxicity properties of CPDP-XT5 was evaluated by performing MTT assay on RPMI 8226 myeloma cell lines. Cell viability results confirmed that XT5 molecules were successfully conjugated to $DSPE-PEG_{2000}-COOH$. Specific targeting properties of CPDP-XT5 NCs and XT5-free NCs (CPDP NCs) were investigated on RPMI 8226 myeloma cell lines by utilizing fluorescent microscopy and results indicated that CPDP-XT5 NCs shows significantly high affinity in comparison to CPDP NCs against the cells. Homology modeling and molecular docking properties of XT5 molecules were evaluated and simulation results confirmed our results.

Supplementary material for this article is available online

---

[7] These authors equally contributed to this work.
[*] Authors to whom any correspondence should be addressed.

(Some figures may appear in colour only in the online journal)

1. Introduction

Early diagnosis of cancer disorders, which is known as a main step of therapy, has attracted the interest of many research groups to develop new strategies especially in non-invasive forms in the last years [1]. In recent years, fluorescent dyes have been widely used as tracing tools in various fields such as diagnosis of cancer cell/tissue and microbial infections for both *in vitro* and *in vivo* conditions [2, 3]. Fluorescent dyes naturally do not exhibit any specific targeting/binding properties against cancer cells therefore further modification progress should be applied [4]. There are various strategies for specifically modifying fluorescent molecules against cancer cells including direct and indirect approaches. In direct modification, fluorescent molecules are chemically modified with functional groups or immobilized to antibodies, aptamers and proteins [5]. Whereas, in indirect modification techniques, fluorescent molecules are targeted/delivered with modified carriers/vectors to the desired cells [6]. As an example to direct modification, de boer *et al* conjugated cetuximab (anti-epidermal growth factor receptor) with near infrared fluorescent dye in order to specific imaging of carcinoma cells. The results indicating successful localization of fluorescently labeled antibodies (cetuximab) onto carcinoma cells [7]. Guan *et al* modified heptamethine cyanine dye with genistein-IR 783, the biologically active flavonoid-based natural product, for bioimaging of MCF-7 cancer cells. The *in-vito* and *in-vivo* stadies shows high affinity of modified dye to MCF-7 compare to non-modified one [8]. Dong *et al* in concept of indirect modification of fluorescent dye, buried the synthetized amphiphilic dye (SQR23) within bilayer region of folic acid (targeting agent) post functionalized liposomes in order to bioimaging of SKOV-3 ovarian cancer cells. Fluorescence observation of SKOV-3 ovarian cancer cells using FA-modified liposomes shows 3-folled increasing in intencity value compare SKOV-3 that treated with unmodified liposomes [9].

Drug delivery systems are known as engineered systems which were developed in the past few decades to deliver therapeutic/diagnostic compounds specifically to the desired cell or tissues with high performance in living systems [10]. For this purpose, drugs or dyes are delivered by using proper vehicles in various forms, sizes and materials based on application area [11, 12]. Although the selection of a drug delivery vehicle can be different depending on the various applications, in biological cases they should be in nano-size and biocompatible nature [13].

Nanotechnology has opened up a new age in drug delivery and diagnosis of cancer and infectious disease applications due to its promising advantages and incredible potential of development [14–16]. Nanoparticles that are known as a fundamental part of nanotechnology, show tremendous potential as an effective drug delivery system [12,

17–19]. Although various materials in nano-size have been commonly used in drug delivery applications, organic nanostructures like liposomes and micelles are preferred due to their novel advantages including low toxicity, high drug/dye packaging capacity and facile modification properties [20, 21].

Nowadays, preparation of nanoparticles enables highly sensitive detection of cancer cells depending on diagnosis strategies which can be performed due to modification of nanoparticle systems via proper ligand molecules (probe) such as antibodies, aptamers, or new generation of receptor sensitive engineered drugs [22–24]. Abedin *et al* used monoclonal antibody to specified synthetized paclitaxel carring trastuzumab-based nanorods against HER2 positive breast cancer cells for induced synergistic treatment purpose. MTT assay results indicated that the antibody specified nanorods significantly induced synergic effects compare to antibody free system [25]. In order to treatment Gynecological Carcinoma Cells, Lopes-Nunes *et al* used AS1411 aptamer to functionalize gold nanoparticles caring acridine orange derivative (as an anticancer agent). Cellular uptake and cell viability results shows the high performances of aptamer to deliver the anticancer caring nanoparticle system to cancer cells [26].

Protease-activated receptors (PARs) are members of the G protein-coupled receptor family [27]. There are four members of the PAR family (PAR1-4). Among of them, PAR1 is the most characterized one [28]. Thrombin as a coagulation protease activates PAR1 receptor through the cleavage of its N-terminal that generates a new N-terminus [29].

PAR1 has been found to be a promising target in the discovery of novel agents against various cancers. Researchers have demonstrated that PAR1 is overexpressed and has a role in many cancers including breast cancer [30], colon cancer [31], prostate cancer [32], kidney cancer, lung cancer and hepatocellular carcinoma [33]. The experimental studies proved that PAR1 can induce proliferation and differentiation of multiple myeloma conditions [34]. Overexpression of PAR1 is also correlated with malignant phenotype [33]. Furthermore, its expression level is proportional with the degree of invasiveness in invasive and metastatic tumors [35]. In another study, its overexpression has been correlated with high level of β-catenin, which is associated with lung cancer, ovarian cancer, endometrial cancer, malignant breast tumors, hepatocellular and colorectal carcinomas [36, 37].

Benzamide derivatives including XT5 were found to have *in vitro* anticancer effects [38]. In our previous study, XT5 was suggested as a novel molecule that has apoptotic effects on imatinib sensitive and resistant K562 cells [39]. In one of our previous studies, it was found that XT5 has a significant PAR1 antagonist activity [34]. The results
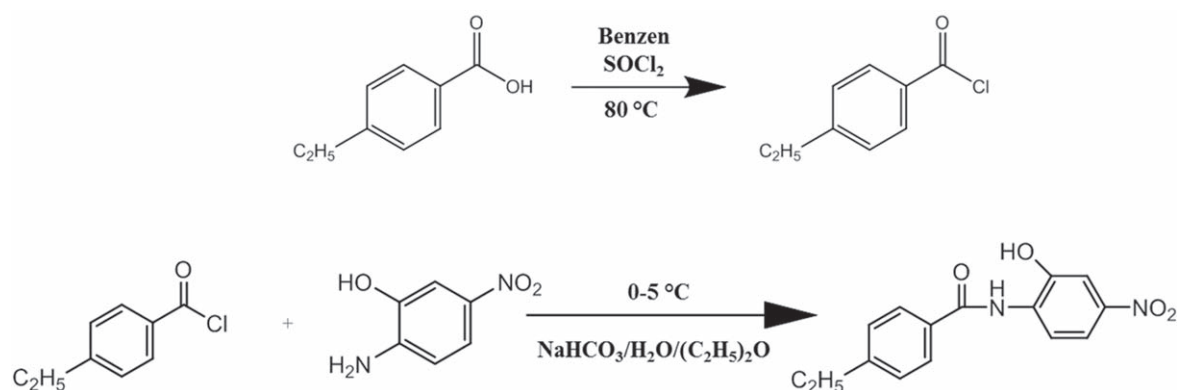
Figure 1. The chemical mechanism of preparation of XT5 molecules.

obtained in our previous studies were supported by molecular modeling analysis [34, 39].

Computational methods play a substantial role in the drug discovery process [40]. Homology modeling and molecular docking are among the computational methods that enable the drug discovery process faster, cheaper and more efficient. Homology modeling is used in the prediction of the 3D structure of proteins from their amino acid sequences [41]. Molecular docking is utilized to generate the binding pose and affinity between ligands and targets by predicting their interactions [42].

In this work, we developed a fluorescence enable XT5-functionalized liposomal-based nanocapsules (NCs) system in order to achieve the specific diagnosis of myeloma cancer cells. For this purpose, DSPE-PEG$_{2000}$-COOH lipid molecules were conjugated with XT5 molecules due to esterification reaction and confirmed by Fourier-Transform Infrared Spectroscopy (FTIR) analysis. PFBT fluorescent-conjugated molecule was encapsulated by DSPE-PEG$_{2000}$-COO-XT5 through ultra-sonication techniques. scanning electron microscopy (SEM), UV–vis and fluorescence spectrophotometry analysis confirmed successful preparation of PFBT-encapsulated DSPE-PEG$_{2000}$-COO-XT5 NCs (CPDP-XT5 NCs) in desired properties. Cytotoxicity of NCs was evaluated by performing MTT assay and results indicated that the developed system has high biocompatibility. Specific targeting properties of XT5-conjugated NCs were also investigated by utilizing fluorescence microscopy. The obtained images indicated that CPDP-XT5 NCs possess significantly high affinity to myeloma cells. Specific targeting properties of our previously synthesized molecule, XT5, was also examined. 3D structure of its potential target, PAR1, was generated by homology modeling. Then, the binding mode and affinity of XT5 to PAR1 was analyzed by molecular docking. In addition, nanoparticle that bears XT5 was prepared and cytotoxic activities of XT5 and XT5 conjugated NCs were also compared.

2. Material and methods

2.1. Synthesis of XT5 molecule

10 mmol of p-ethyl benzoic acid was refluxed with 2 ml SOCl$_2$ (Sigma-Aldrich, USA) and 5 ml benzene (Sigma-Aldrich, USA)

at 80 °C for 4–5 h. At the end of the reaction, benzene and SOCl$_2$ were blown off using rotavapor and the residue was dissolved in 10 ml of diethylether (Sigma-Aldrich, USA). In another flask, 10 mmol of 2-amino-5-nitro phenol (Sigma-Aldrich, USA) and 20 mmol of NaHCO$_3$ (Sigma-Aldrich, USA) were dissolved in 10 ml of distilled water and 10 ml of diethylether. The obtained solution was added to the substance obtained in the previous step. The mixture was rotated in an ice bath overnight and filtered through plain filter paper and washed sequentially with distilled water, 2N HCl (Sigma-Aldrich, USA), distilled water and diethylether. Finally, the obtained solution was crystallized with ethanol and activated charcoal [43]. The chemical mechanism of the preparation of XT5 molecules was shown in figure 1.

2.2. Preparation and characterization of DSPE-PEG$_{2000}$-XT5 conjugate

In order to specific targeting of NCs against myeloma cells, NCs were functionalized with XT5 by condensation reaction between the hydroxyl groups of XT5 and carboxyl-terminated lipid. For this purpose, 5 mg of DSPE-PEG$_{2000}$-COOH (1.8 μmol) (Sigma-Aldrich, USA) as an encapsulation material, 1.5 mg of XT5 (5.4 μmol) and 0.55 mmol of 4-Dimethylaminopyridine (DMAP) (Sigma-Aldrich, USA) were dissolved in 2 ml of tetrahydrofuran (THF) (Sigma-Aldrich, USA), and cooled at −10 °C (ice/NaCl bath) under stirring. 5.55 mmol of dicyclohexylcarbodiimide (DCC) (Sigma-Aldrich, USA) was dissolved in THF and added dropwise to the previously prepared solution and the reaction mixture was stirred at −10 °C under N$_2$ atmosphere. The consumption of DCC in the reaction medium was monitored by decreasing kinetic of the 2110 cm^{-1} infrared characteristic peak of N=C=N moiety using FT-IR spectroscopy (Nicolet™ iS™ 10 FTIR Spectrometer-Thermo Fisher Scientific, USA). At the end of the condensation reaction, filtration was used to remove the insoluble side product dicyclohexylurea. Finally, after filtration, THF was removed in a rotary evaporator and the solid phase repeatedly dissolved/precipitated with DCM/n-hexane in order to completely remove undesired dicyclohexylurea from the environment. The obtained DSPE-PEG$_{2000}$-COO-XT5 was dried under a vacuum oven and kept at −20 °C. The characterization of the prepared

DSPE-PEG$_{2000}$-COO-XT5 conjugate was carried out by utilizing FT-IR and ^{1}H NMR spectroscopies (Bruker 400 MHz AV, USA).

2.3. Preparation of fluorescence enables DSPE-PEG$_{2000}$-COO-XT5 NCs (CPDP-XT5 NCs)

The preparation of fluorescence label carrying NCs with desired targeting properties against PAR1 receptors, PFBT conjugated polymer (CP) (Sigma-Aldrich, USA) was encapsulated according to the protocol which was previously reported by the author [44]. For this purpose, 1 mg of DSPE-PEG$_{2000}$-COOH and 2 mg of synthetized DSPE-PEG$_{2000}$-COO-XT5 molecules were dissolved in 1 ml of THF. In parallel, 1 mg of PFBT molecule was dissolved in 1 ml of THF and added to the previous solution. The prepared solution was added to 9 ml of distilled water and sonicated for 60 s with a 12 W probe sonicator (Bandelin SONOPULS HD 2200, Sigma, USA). The mixture was stirred in dark conditions overnight in order to remove THF residues from the aqueous solution. The obtained solution was centrifuged at 3000 g for 15 min and the supernatant was collected and filtered by using 0.2 μm syringe filtration. The CPDP-XT5 NCs solution was dialyzed (cut-off: 30 KDa) overnight to remove possible impurities and non-immobilized XT5 molecules.

Absorption, excitation, and emission properties of prepared NCs were investigated by using a fluorescence spectrophotometer (CARY ECLIPSE, Australia) and UV–vis spectrophotometer (SHIMADZU UV-1800, Japan). The morphologic properties of NCs were visualized by utilizing SEM (Zeiss Sigma 300, France). The size and charge stability of nanocapsuls in different solutions including D.W., P.B.S. and culture medium were avaluted by employing a zeta potential (Malvern, USA).

2.4. Cell viability tests

The cytotoxicity properties of XT5, CPDP NCs and CPDP-XT5 NCs were investigated by performing MTT technique. For this purpose, RPMI 8226 cells were cultured in 96-well plates at 10.000 cells/well seeding density in 100 μl of RPMI-1640 medium (Gibco, NY, USA) with 10% fetal bovine serum (Hao Yang, China). Cells were exposed to various concentrations (0, 0.8125, 1.625, 3.25, 7, 5 and 15 pM) of XT5, CPDP NCs and CPDP-XT5 NCs. Then, the plates were incubated in a 5% CO$_2$ humidified incubator at 37 $^\circ$C for 72 h.

After 72 h, the medium was removed from wells and washed with PBS and replaced with initial amount of the fresh medium. 10 μl of 3-(4,5-dimethylthiazol-2-yl)-2,5-diphenyltetrazolium bromide salt (MTT agent) (Sigma-Aldrich, USA) was added to the cells at a concentration of 5 mg ml^{-1} and incubated for 2 h at 37 $^\circ$C. Then, 100 μl of MTT solvent solution was added and incubated at 37 $^\circ$C overnight. After overnight incubation, 96-well plates were measured by utilizing spectrophotometer (Biotek, Epoch USA) at 550 and 690 nm to evaluate cell viability. The absorbance values of free cells was accepted as 100% viability and the viability in other cell groups (XT5, CPDP NCs and CPDP-XT5 NCs) were calculated as percentage based on this value.

2.5. Investigation of specific targeting properties of CPDP-XT5 NCs

10 000 cells of myeloma cancer cell line was added to each well containing 100 μl of medium. The cells were separately exposed to equal concentration of CPDP NCs and CPDP-XT5 NCs and then incubated at 37 $^\circ$C for 1 h, thus allowing time for NCs to interact with the PAR receptor of the cells. The specific attachment of CPDP-XT5 NCs to PAR1 receptor of myeloma cancer cells was determined by using fluorescence microscope (Olympus BX51, America). The bonding properties of CPDP NCs was investigated as a negative control group.

2.6. Homology modeling

The PAR1 sequence retrieved from UniProt (accession number: P25116) was used in the modeling [45]. Protein BLAST search was performed by setting the database as PDB (protein data bank). Then, homology modeling was undertaken using MODELLER [46], and I-TASSER [47]. The generated models were compared and the model with relatively high quality was selected. Validation and verification of the best model was performed with SAVES [48]. The binding site of the model was predicted using CASTp [49].

2.7. Molecular docking

Molecular docking was performed with AutoDock Vina. [50] Prior to docking, GRID map of the model was determined. The model generated was prepared by adding polar hydrogens and assigning Gasteiger charges. The ligand (XT5) was drawn using ChemDraw ultra 12 [51]. The ligand was prepared by minimizing its energy, adding polar hydrogens and assigning Gasteiger charges. After assigning the receptor, the ligand and the size as well as the center of the GRID map, the command prompt of AutoDock Vina was run [50]. The receptor-ligand interactions of the docking results were visualized and analyzed by using Discovery Studio 3.5 [52]. To validate and compare the molecular docking results, the same procedure was applied on two reference ligands that are PAR1 inhibitors, Atopaxar and Vorapaxar.

3. Results and discussion

Conjugation performance of XT5 to DSPE-PEG$_{2000}$-COOH molecules was evaluated using FTIR spectroscopy. For comparison purposes, between DSPE-PEG$_{2000}$-COOH and its conjugated form, FTIR spectra were obtained for DSPE-PEG$_{2000}$-COOH and DSPE-PEG$_{2000}$-COO-XT5 (figure 2). The appearance of a new peak after conjugation reaction at 1614 cm^{-1}, 1508 cm^{-1} and 1470 cm^{-1} (characteristic band of C–C stretching vibration of aromatic ring in XT5) confirmed that esterification reaction was
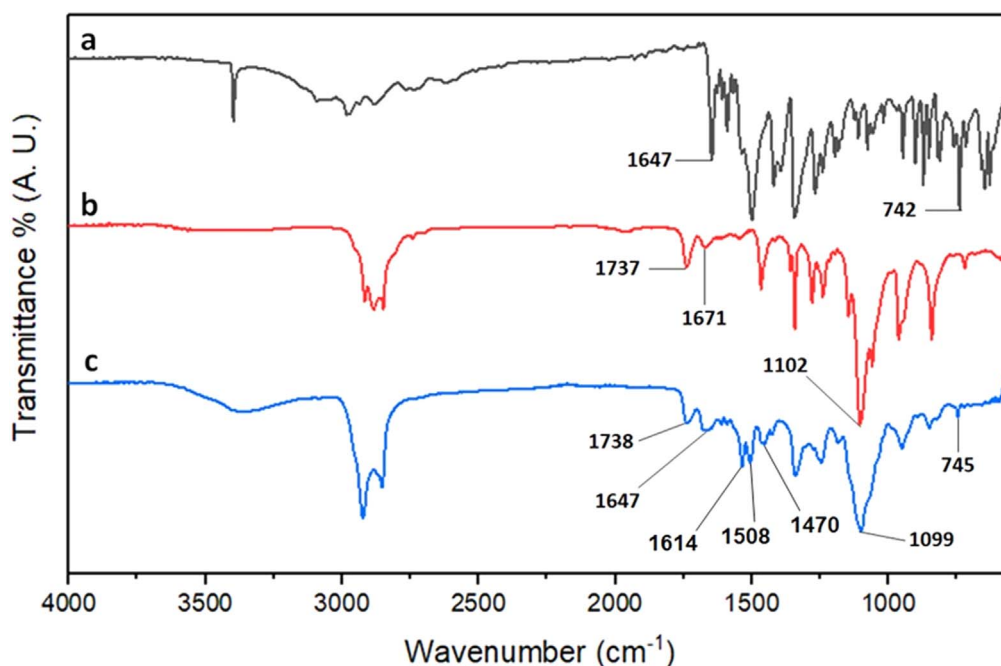
Figure 2. Representative FTIR spectra of (a) XT5, (b) DSPE-PEG$_{2000}$-COOH) and (c) DSPE-PEG$_{2000}$-COO-XT5 molecules.

Table 1. Bond assignment of synthetized DSPE-PEG$_{2000}$-COO-XT5 conjugate.

Wavenumber (cm^{-1})	Chemical bound	References
745	N–H twisting of amide bond	[53]
1100	C–O stretching vibration	[54]
1641	C–C stretching vibration of aromatic ring	[55]
1671	C=O stretching vibration	[56]
1737	C=O stretching vibration (ester)	[57]

successfully performed between free carboxyl group of DSPE-PEG$_{2000}$-COOH and hydroxyl group of XT5 molecules. The bound assignments of obtained FTIR spectra of XT5, DSPE-PEG$_{2000}$-COOH and DSPE-PEG$_{2000}$-COO-XT5 are shown in table 1.

In order to confirm conjugation of XT5 to DSPE-PEG$_{2000}$-COOH molecule, 1H NMR was performed and obtained spectra related to XT5, DSPE-PEG$_{2000}$-COOH and DSPE-PEG$_{2000}$-XT5 conjugated was shown in figure 3. The peak at 2.69 ppm corresponds to the methyelene group of XT5, whereas the 7.26–7.89 ppm peak atribitued to the benzene ring of XT5 (figure 3(a)). The characteristic benzene peak ring was present in the DSPE-PEG$_{2000}$-COOH spectrum (figure 3(b)). The NMR spectrum of DSPE-PEG$_{2000}$- XT5 demonstrated that aromatic ring protons peaks shifted upfield as hydroxy group were replaced by ester linkage (figure 3(c)). In other words, there were benzene rings with new chemical envernement in DSPE-PEG$_{2000}$-XT5, indicating successful conjugation of XT5 to DSPE-PEG$_{2000}$-COOH.

The excitation and emission properties of the fabricated CPDP-XT5 NCs were determined by utilizing UV–vis and fluorescence spectrophotometer. The results indicated that CPDP-XT5 NCs exhibited two absorbance peaks at 340 and 460 nm with emission at 560 nm (figure 4(a)). In addition, it is shown in figure 4(b) that the fabricated CPDP-XT5 NCs exhibited strong yellow fluorescence emission under UV light exposure at 365 nm. The obtained NCs had strong yellowish fluorescence emission under UV exposure at 365 nm. The morphologic properties of NCs were determined by using SEM and the images demonstrated that CPDP-XT5 NCs were synthetized in spherical morphology with size distribution of ∼80 nm (figure 4(c)). The size distribiton and zata potantial properties of CPDP-XT5 NCs in D.W., P.B.S. and culture medium were measured and size and potantial were obtained to be ∼85 nm and −25.5 mV without any significant changes in the used solutions (figures SI (1) and (2) (available online at stacks.iop.org/NANO/33/265101/mmedia)). This should be noted that the similar values were obtained after one month by Zeta-potantial mesurements.

The biocompatibility properties of XT5, CPDP NCs and CPDP-XT5 NCs were determined by using conventional MTT assay. Therefore, we performed cytotoxicity tests by the exposure of RPMI 8226 cells with various concentrations of XT5, CPDP NCs and CPDP-XT5 NCs. The dose-dependent proliferation of cells was evaluated after 72 h. For the case of the XT5 molecule, after 72 h of treatment, cell viability of >80% was detected at the maximum concentration (15 pM) (figure 5(a)). The decrease in cell viability indicated that the XT5 molecule shows desired affinity to PAR1 receptors. The reason could be overexpression of PAR receptors in cancer cells compared to normal cells [58, 59]. The cytotoxicity of the CPDP NCs was evaluated and the results indicated high biocompatibility of fabricated NCs with cell viability of >100%. The CPDP NCs exhibited similar molecular structure with cell membrane that enable NCs to integrate into the cell membrane and improve cell proliferations [44]. Cell
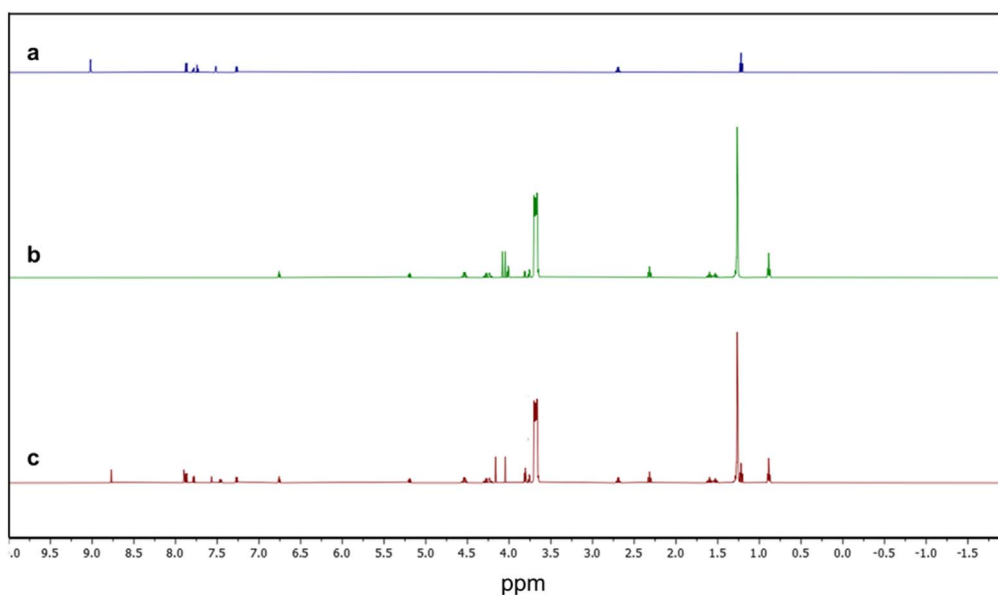
Figure 3. Representetive ^{1}H NMR spectra of (a) XT5, (b) DSPE-PEG$_{2000}$-COOH and (c) DSPE-PEG$_{2000}$-XT5.
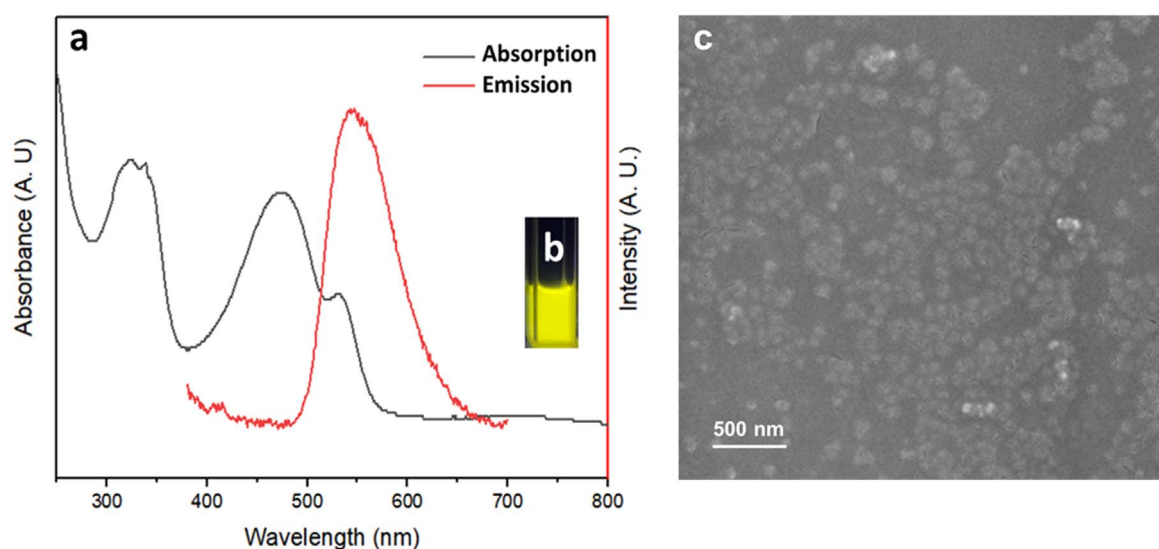
Figure 4. (a) Absorption and emission properties of fabricated CPDP-XT5 NCs, (b) fluorescence emission of CPDP-XT5 NCs under 365 nm UV light exposure, and (c) SEM imaging of CPDP-XT5 NCs.

viabilities of synthetized CPDP-XT5 NCs were also evaluated and results exhibited similar values to the XT5. This results clearly proved that XT5 molecule was successfully conjugated to DSPE-PEG$_{2000}$-COOH molecule.

Specific binding/targeting properties of CPDP-XT5 NCs to myeloma cancer cell line was determined via fluorescence microscopy. As shown in figures 4(d) and (e), in the presence of CPDP-XT5 NCs system, significant fluorescence signals were observed for myeloma cancer cell. Therefore, as expected, the XT5 free CPDP NCs did not exhibit any specific binding properties to myeloma cancer cell (figures 5(b) and (c)). The results indicated that our proposed NC system can be used for detection of myeloma cancer cells similar to the reports available in literature [60, 61]. This should be noted that the binding/targeting properties against cells with low PAR1 receptor expression was previously investigated in

our group and resultas shows low binding properties compare to highly expressed PAR1 receptor cellas like as myeloma cancer cells [62].

3.1. Homology modeling

BLAST search of the protein structure with PDB ID 3VW7 was found to give the highest similarity with the used sequence. The A chain of 3VW7 was revealed to have 73% coverage (81% coverage after the propeptide was cleaved) and 99.07% identity with the PAR1 sequence. Homology modeling is considered as a reliable method for computational structure prediction [41]. Thus, the structure of PAR1 was generated using homology modeling. From the validation and verification analysis, the model was demonstrated to have 96% ERRAT quality factor, 87% Verify 3D value and 97% of
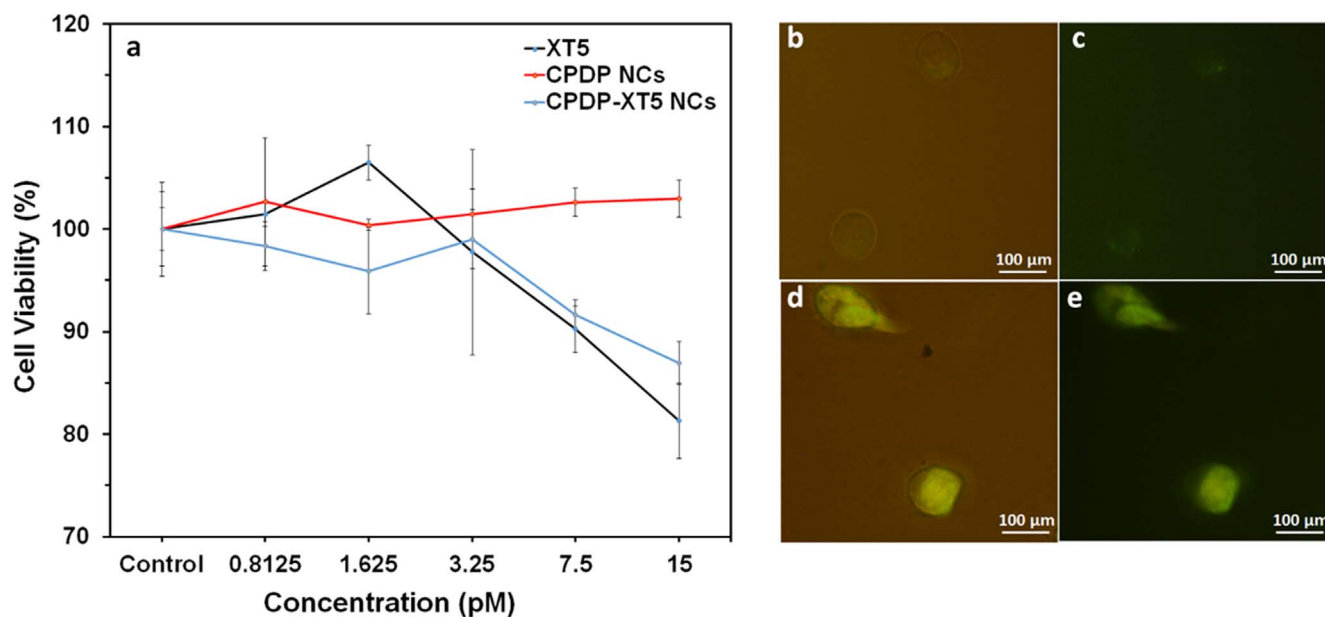
Figure 5. (a) Cell viability of XT5, CPDP NCs and CPDP-XT5 NCs on RPMI 8226 cell line, (b) and (c) fluorescence imaging of RPMI 8226 cells treated with CPDP NCs, and (d) and (e) fluorescence imaging of RPMI 8226 cells treated with CPDP-XT5 NCs.
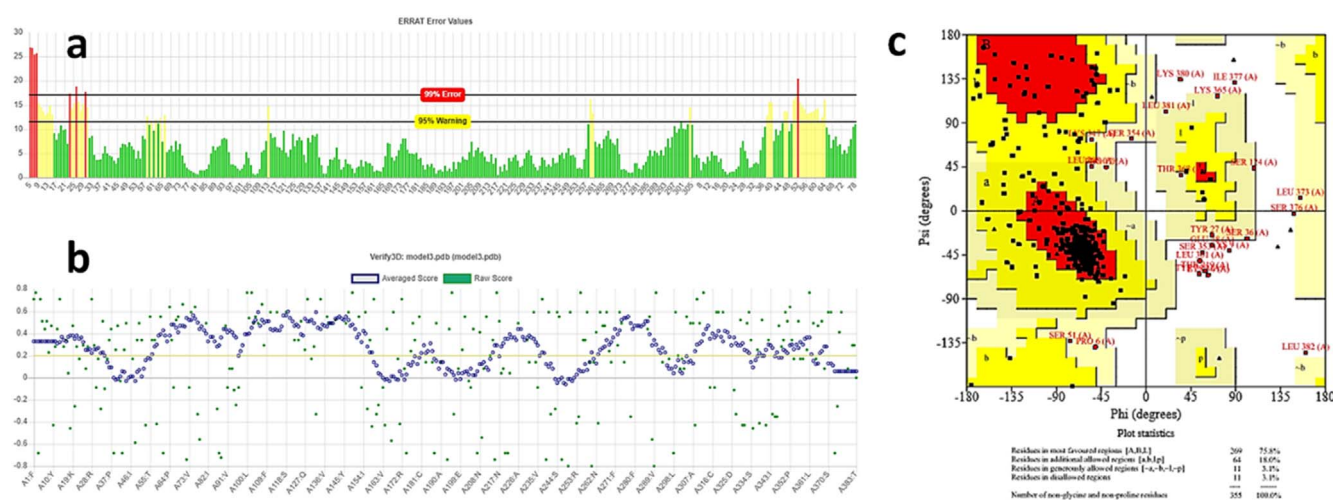
Figure 6. Validation and verification results of the model. (a) ERRAT quality factor (96%), (b) verify 3D value (87%) and (c) Ramachandran plot (97% in the allowed region).

the residues was in the allowed region of the Ramachandran plot (figure 6). The results showed that the generated model is reliable enough.

Molecular docking was carried out with the generated model (figure 7(a)). The binding site of the model was estimated with CASTp before docking (figure 7(b)).

3.2. Molecular docking

After the GRID map was determined in a way that covers the binding region (figure 8(b)), molecular docking of the model with ligands was performed with AutoDock Vina. Molecular docking results demonstrated that XT5 interacted with PAR1 model through hydrogen bonds at Asp214, Leu216, Tyr225, His294 and alkyl–alkyl (pi) interactions at Ileu46 and Val204

positions (figure 8(a)). The interactions were found to have similarity with the reference ligands, Atopaxar and Vorapaxar (table 2). The interactions at Leu216, Asp214 and Tyr225 were common to XT5 and Atopaxar. In addition, the two interactions at Ileu46 were common to XT5 and Vorapaxar (figure 8(c)). Furthermore, the binding energies of the docked molecules were similar (table 2). Computational analysis of the interactions of XT5 and similar derivatives with PAR1 was performed in our previous studies using the structure of 3VW7, which covers 70% of the PAR1 sequence. Molecular docking results were found to have fewer hydrogen bond interactions than the results obtained in a previous study [34]. This might be resulted from lack of some parts of the amino acid sequence in the structure used in previous studies. Thus, the molecular docking analysis performed by generating the
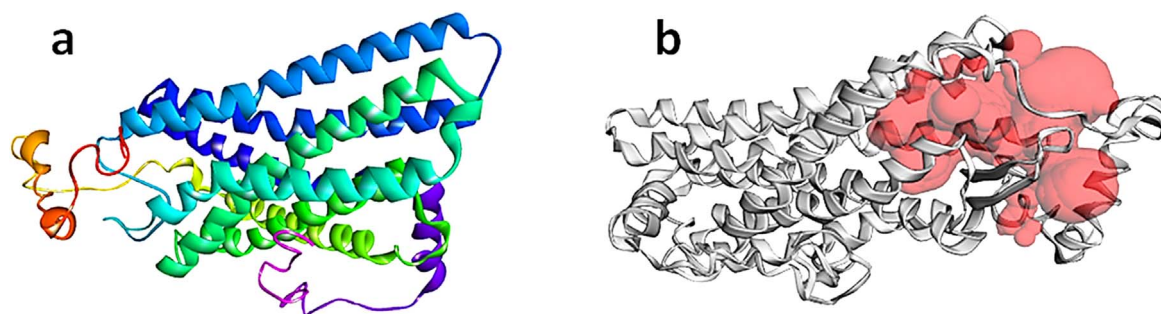
Figure 7. (a) 3D structure of the generated model and (b) predicted binding region of the model.
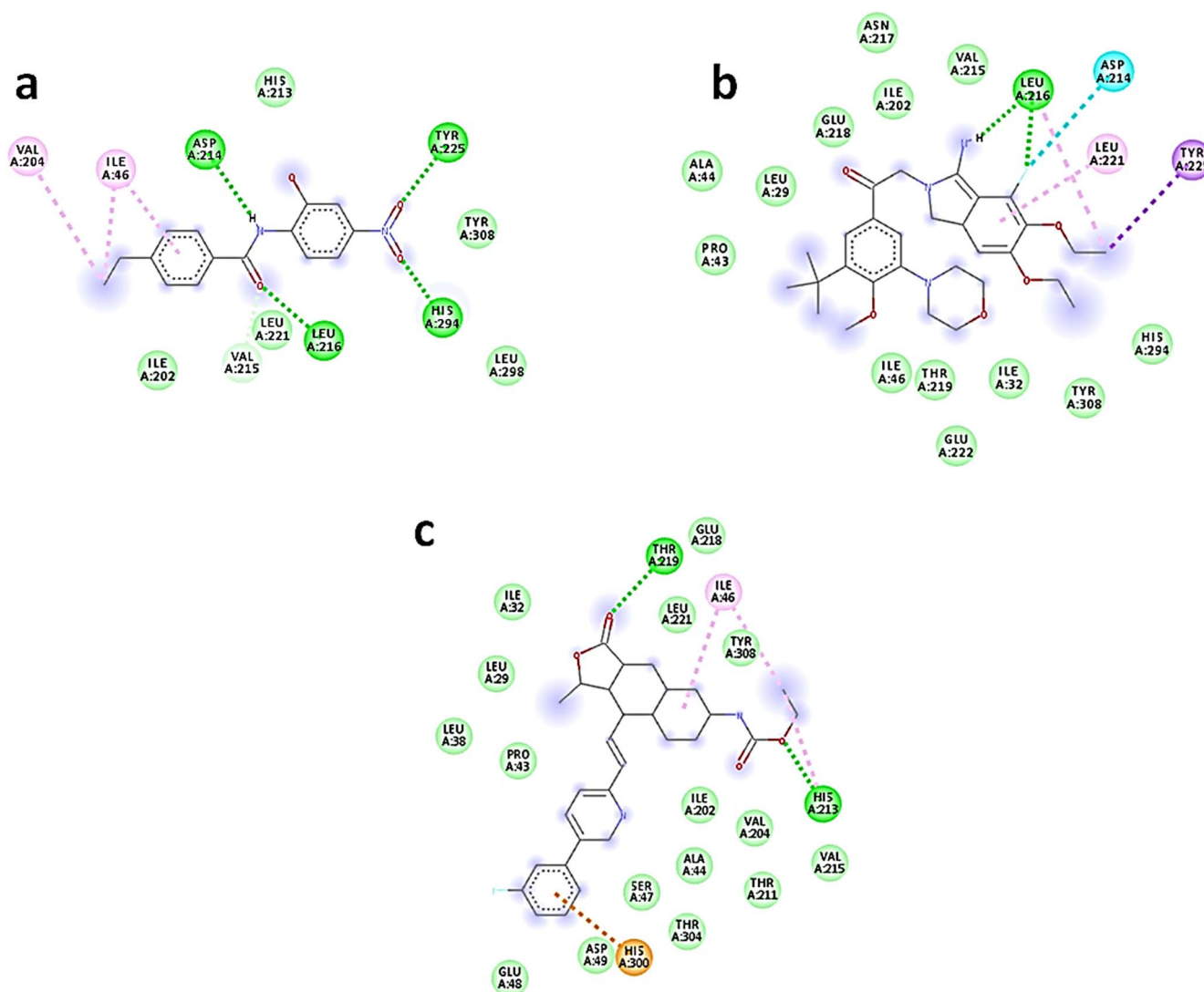
Figure 8. Binding profile of (a) XT5, (b) Atopaxar and (c) Vorapaxar with the prepared model.

Table 2. Comparison of the interactions of the reference ligands (Atopaxar, Vorapaxar) and XT5 with the model (common residues are written in bold).

Ligands	Binding energy (kcal mol^{-1})	Hydrogen bond interactions	Other amino acid interactions
Atopaxar	−7.8	Leu216 (2)	Asp214, Leu221, Tyr225
Vorapaxar	−8.6	His213, Thr219	Ile46 (2), His300
XT5	−9.7	Asp214, Leu216, Tyr225, His294	Ile46 (2), Val204

3D structure of the full sequence was resulted in better interactions. The computational analysis revealed that XT5 can bind and thus inhibit PAR1. Therefore, the computational results indicated that XT5 had high affinity towards PAR1, which confirmed the MTT assay results.

4. Conclusion

Early diagnosis plays a vital role in combating cancer. Hence, in this study, PFBT fluorescent-conjugated molecule was encapsulated by DSPE-PEG$_{2000}$-COO-XT5 NCs to come up with a novel way for early diagnosis of myeloma cancer cells. The characteristics of the prepared molecules were found to meet the required conditions as confirmed by SEM, UV–vis and fluorescence spectrophotometry. Cytotoxicity analysis of NCs through MTT assay exhibited that the developed system had high biocompatibility. Furthermore, fluorescence microscopy investigation of CPDP-XT5 NCs indicated that they had high specific affinity towards myeloma cells.

The potential mechanism of action for XT5 was elucidated through homology modeling and molecular docking. A reliable 3D structure of the potential target, PAR1, was built by homology modeling. After that, the binding region was predicted and then binding mode and affinity of XT5 to PAR1 was analyzed by molecular docking. The molecular docking outcomes showed that XT5 could bind to PAR1 similar to the standard drugs. Hence, the computational analysis demonstrated that the specific affinity towards myeloma cells might result from XT5's affinity towards PAR1.

Data availability statement

All data that support the findings of this study are included within the article (and any supplementary files).

Declaration of competing interest

No potential conflict of interest was reported by the authors.

ORCID iDs

Araz Norouz Dizaji https://orcid.org/0000-0001-6720-2115
Ilyas Inci https://orcid.org/0000-0001-7231-7822

References

[1] Chen X et al 2020 Non-invasive early detection of cancer four years before conventional diagnosis using a blood test Nat. Commun. 11 1–10

[2] Luo S, Zhang E, Su Y, Cheng T and Shi C 2011 A review of NIR dyes in cancer targeting and imaging Biomaterials 32 7127–38

[3] Gao L et al 2021 Fluorescent probes for bioimaging of potential biomarkers in Parkinson's disease Chem. Soc. Rev. 50 1219–50

[4] Guo L et al 2020 A side-chain engineering strategy for constructing fluorescent dyes with direct and ultrafast self-delivery to living cells Chem. Sci. 11 661–70

[5] Cheng W, Chen H, Liu C, Ji C, Ma G and Yin M 2020 Functional organic dyes for health-related applications View 1 20200055

[6] Klymchenko A S, Liu F, Collot M and Anton N 2021 Dye-loaded nanoemulsions: biomimetic fluorescent nanocarriers for bioimaging and nanomedicine Adv. Healthc. Mater. 10 2001289

[7] De Boer E et al 2015 In vivo fluorescence immunohistochemistry: localization of fluorescently labeled cetuximab in squamous cell carcinomas Sci. Rep. 5 1–11

[8] Guan Y et al 2019 Synthesis and biological evaluation of genistein-IR783 conjugate: cancer cell targeted delivery in MCF-7 for superior anti-cancer therapy Molecules 24 4120

[9] Dong S, Teo J D W, Chan L Y, Lee C-L K and Sou K 2018 Far-red fluorescent liposomes for folate receptor-targeted bioimaging ACS Appl. Nano Mater. 1 1009–13

[10] Pinelli F, Ortolà Ó F, Makvandi P, Perale G and Rossi F 2020 In vivo drug delivery applications of nanogels: a review Nanomedicine 15 2707–27

[11] Mitchell M J, Billingsley M M, Haley R M, Wechsler M E, Peppas N A and Langer R 2021 Engineering precision nanoparticles for drug delivery Nat. Rev. Drug Discovery 20 101–24

[12] Patra J K et al 2018 Nano based drug delivery systems: recent developments and future prospects J. Nanobiotechnol. 16 1–33

[13] Sung Y K and Kim S W 2020 Recent advances in polymeric drug delivery systems Biomater. Res. 24 1–12

[14] Türeli N G and Türeli A E 2020 Upscaling and GMP production of pharmaceutical drug delivery systems Drug Deliv. Trends (Amsterdam, Netherlands: Elsevier) 215–29

[15] Dizaji A N, Ozek N S, Yilmaz A, Aysin F and Yilmaz M 2021 Gold nanorod arrays enable highly sensitive bacterial detection via surface-enhanced infrared absorption (SEIRA) spectroscopy Colloids Surf. B 206 111939

[16] Dizaji A N, Ozek N S, Aysin F, Calis A, Yilmaz A and Yilmaz M 2021 Combining vancomycin-modified gold nanorod arrays and colloidal nanoparticles as a sandwich model for the discrimination of Gram-positive bacteria and their detection via surface-enhanced Raman spectroscopy (SERS) Analyst 146 3642–53

[17] Deng Y et al 2020 Application of the nano-drug delivery system in treatment of cardiovascular diseases Front. Bioeng. Biotechnol. 7 489

[18] Sim S and Wong N K 2021 Nanotechnology and its use in imaging and drug delivery Biomed. Rep. 14 1–9

[19] Sezgin-Bayindir Z, Losada-Barreiro S, Bravo-Díaz C, Sova M, Kristl J and Saso L 2021 Nanotechnology-based drug delivery to improve the therapeutic benefits of NRF2 modulators in cancer therapy Antioxidants 10 685

[20] Witika B A et al 2020 Biocompatibility of biomaterials for nanoencapsulation: current approaches Nanomaterials 10 1649

[21] Guimarães D, Cavaco-Paulo A and Nogueira E 2021 Design of liposomes as drug delivery system for therapeutic applications *Int. J. Pharm.* **601** 120571

[22] He F *et al* 2020 Aptamer-based targeted drug delivery systems: current potential and challenges *Curr. Med. Chem.* **27** 2189–219

[23] Arslan F B, Atar K O and Calis S 2021 Antibody-mediated drug delivery *Int. J. Pharm.* **596** 120268

[24] Khot V M, Salunkhe A B, Pricl S, Bauer J, Thorat N D and Townley H 2020 Nanomedicine-driven molecular targeting, drug delivery, and therapeutic approaches to cancer chemoresistance *Drug Discovery Today* **26** 726–39

[25] Abedin M R, Powers K, Aiardo R, Barua D and Barua S 2021 Antibody–drug nanoparticle induces synergistic treatment efficacies in HER2 positive breast cancer cells *Sci. Rep.* **11** 1–17

[26] Lopes-Nunes J *et al* 2021 Aptamer-functionalized gold nanoparticles for drug delivery to gynecological carcinoma cells *Cancers* **13** 4038

[27] Vu T-K H, Hung D T and Wheaton V I 1991 Coughlin Sr Molecular cloning of a functional thrombin receptor reveals a novel proteolytic mechanism of receptor activation *Cell* **64** 1057–68

[28] O'Brien P J, Molino M, Kahn M and Brass L F 2001 Protease activated receptors: theme and variations *Oncogene* **20** 1570–81

[29] Gieseler F, Ungefroren H, Settmacher U, Hollenberg M D and Kaufmann R 2013 Proteinase-activated receptors (PARs)– focus on receptor-receptor-interactions and their physiological and pathophysiological impact *Cell Commun. Signaling* **11** 1–26

[30] Chu H-W *et al* 2014 A novel estrogen receptor-microRNA 190a-PAR-1-pathway regulates breast cancer progression, a finding initially suggested by genome-wide analysis of loci associated with lymph-node metastasis *Hum. Mol. Genet.* **23** 355–67

[31] Gratio V *et al* 2010 Kallikrein-related peptidase 4: a new activator of the aberrantly expressed protease-activated receptor 1 in colon cancer cells *Am. J. Pathol.* **176** 1452–61

[32] Chay C H *et al* 2002 A functional thrombin receptor (PAR1) is expressed on bone-derived prostate cancer cell lines *Urology* **60** 760–5

[33] Han N, Jin K, He K, Cao J and Teng L 2011 Protease-activated receptors in cancer: a systematic review *Oncol. Lett.* **2** 599–608

[34] Hidayat A *et al* 2015 Insight into human protease activated receptor-1 as anticancer target by molecular modelling *SAR QSAR Environ. Res.* **26** 795–807

[35] Garcia-Lopez M T, Gutiérrez-Rodríguez M and Herranz R 2010 Thrombin-activated receptors: promising targets for cancer therapy? *Curr. Med. Chem.* **17** 109–28

[36] Morin P J 1999 β-catenin signaling and cancer *Bioessays* **21** 1021–30

[37] Turm H, Maoz M, Katz V, Yin Y-J, Offermanns S and Bar-Shavit R 2010 Protease-activated receptor-1 (PAR1) acts via a novel Gα13-dishevelled axis to stabilize β-catenin levels *J. Biol. Chem.* **285** 15137–48

[38] Musdal Y *et al* 2012 Inhibition of human glutathione transferase P1-1 by novel benzazole derivatives *Turk. J. Biochem./Turk Biyokimya Dergisi* **37** 419–40

[39] Ozkan T, Hekmatshoar Y, Ertan-Bolelli T, Hidayat A N, Beksac M, Aki-Yalcin E *et al* 2018 Determination of the apoptotic effect and molecular docking of benzamide derivative XT5 in K562 cells *Anti-Cancer Agents in Medicinal Chemistry (Formerly Current Medicinal Chemistry-Anti-Cancer Agents)* **18** 1521–30

[40] Barril X 2017 Computer-aided drug design: time to play with novel chemical matter *Expert Opin. Drug Discovery* **12** 977–80

[41] Muhammed M T and Aki-Yalcin E 2019 Homology modeling in drug discovery: overview, current applications, and future perspectives *Chem. Biol. Drug Des.* **93** 12–20

[42] Chen Y-C 2015 Beware of docking! *Trends Pharmacol. Sci.* **36** 78–95

[43] Ertan T *et al* 2007 Synthesis and biological evaluation of new N-(2-hydroxy-4 (or 5)-nitro/aminophenyl) benzamides and phenylacetamides as antimicrobial agents *Bioorg. Med. Chem.* **15** 2032–44

[44] Norouz Dizaji A, Ding D, Kutsal T, Turk M, Kong D and Piskin E 2020 *In vivo* imaging/detection of MRSA bacterial infections in mice using fluorescence labelled polymeric nanoparticles carrying vancomycin as the targeting agent *J. Biomater. Sci.* Polymer Edition **31** 293–309

[45] Consortium U 2010 Ongoing and future developments at the universal protein resource *Nucleic Acids Res.* **39** D214–9

[46] Kuntal B K, Aparoy P and Reddanna P 2010 EasyModeller: a graphical interface to MODELLER *BMC Res. Notes* **3** 1–5

[47] Yang J, Yan R, Roy A, Xu D, Poisson J and Zhang Y 2015 The I-TASSER Suite: protein structure and function prediction *Nat. Methods* **12** 7–8

[48] Colovos C and Yeates T O 1993 Verification of protein structures: patterns of nonbonded atomic interactions *Protein Sci.* **2** 1511–9

[49] Joe Dundas Z, Jeffery T, Andrew B, Yaron T and Jie L 2006 CASTp: computed atlas of surface topography of proteins with structural and topographical mapping of functionally annotated resiudes *Nucleic Acids Res.* **34** W116–8

[50] Trott O and Olson A J 2010 AutoDock Vina: improving the speed and accuracy of docking with a new scoring function, efficient optimization, and multithreading *J. Comput. Chem.* **31** 455–61

[51] Cousins K R 2011 *Comput. Rev. ChemDraw Ultra 12.0* (Columbus, OH: ACS Publications) (https://doi.org/ 10.1021/ja204075s)

[52] Barnum D, Greene J, Smellie A and Sprague P 1996 Identification of common functional configurations among molecules *J. Chem. Inf. Comput. Sci.* **36** 563–71

[53] Devendiran M, Kumar K K and Narayanan S S 2017 Fabrication of a novel Ferrocene/Thionin bimediator modified electrode for the electrochemical determination of dopamine and hydrogen peroxide *J. Electroanal. Chem.* **802** 78–88

[54] Abdelrazek E, Elashmawi I, El-Khodary A and Yassin A 2010 Structural, optical, thermal and electrical studies on PVA/ PVP blends filled with lithium bromide *Curr. Appl Phys.* **10** 607–13

[55] Qi F *et al* 2017 Efficient organic–inorganic intumescent interfacial flame retardants to prepare flame retarded polypropylene with excellent performance *RSC Adv.* **7** 31696–706

[56] Srikanth C S and Chuang S S 2012 Spectroscopic investigation into oxidative degradation of silica-supported amine sorbents for CO_2 capture *Chem. Sus. Chem.* **5** 1435

[57] Balogun A O, Lasode O A, Li H and McDonald A G 2015 Fourier transform infrared (FTIR) study and thermal decomposition kinetics of sorghum bicolour glume and albizia pedicellaris residues *Waste Biomass Valorization* **6** 109–16

[58] Garcia-Bates T M, Bernstein S H and Phipps R P 2008 Peroxisome proliferator-activated receptor γ overexpression suppresses growth and induces apoptosis in human multiple myeloma cells *Clin. Cancer Res.* **14** 6414–25

[59] Edis Z, Wang J, Waqas M K, Ijaz M and Ijaz M 2021 Nanocarriers-mediated drug delivery systems for anticancer agents: an overview and perspectives *Int. J. Nanomed.* **16** 1313

[60] Kiziltepe T *et al* 2012 Rationally engineered nanoparticles target multiple myeloma cells, overcome cell-adhesion-

mediated drug resistance, and show enhanced efficacy *in vivo Blood Cancer J.* **2** e64–64

[61] Detappe A, Reidy M, Ghoroghchian P P and Ghobrial I M 2017 *Development of an Antibody-Targeted Nanoparticle Early Detection Minimal Residual Disease in Multiple Myeloma* (Washington, DC: American Society of

Hematology) (https://doi.org/10.1182/blood.V130. Suppl_1.4430.4430)

[62] Beksac M *et al* 2015 Expression and *in vitro* binding of protease activated receptor1 (PAR1) with novel anti-PAR1 molecules: data on fresh myeloma marrow plasma cells and human myeloma cell lines *Blood* **126** 4440